Eur. Phys. J. A **6**, 391–397 (1999)

THE EUROPEAN PHYSICAL JOURNAL A

Observation of superdeformed states in ^{88}Mo

T. Bäck[1], B. Cederwall[1], R. Wyss[1], A. Johnson[1], J. Cederkäll[1,a], M. Devlin[2], J. Elson[2], D.R. LaFosse[2,b], F. Lerma[2], D.G. Sarantites[2], R.M. Clark[3], P. Fallon[3], I.Y. Lee[3], A.O. Macchiavelli[3], R.W. Macleod[3]

[1] Department of Physics, Royal Institute of Technology, 104 05 Stockholm, Sweden
[2] Chemistry Department, Washington University, St. Louis, MO 63130, USA
[3] Nuclear Science Division, Lawrence Berkeley Laboratory, Berkeley, CA, USA 94720

Received: 20 May 1999 / Revised version: 25 August 1999
Communicated by J. Äystö

Abstract. High-spin states in ^{88}Mo were studied using the GAMMASPHERE germanium detector array in conjunction with the MICROBALL CsI(Tl) charged-particle detector system. Three γ-ray cascades with dynamic moments of inertia showing similar characteristics to superdeformed rotational bands observed in the neighbouring $A = 80$ region have been identified and assigned to the nucleus ^{88}Mo. The quadrupole moment of the strongest band, deduced by the Residual Doppler Shift Method, corresponds to a quadrupole deformation of $\beta_2 \approx 0.6$. This confirms the superdeformed nature of this band. The experimental data are interpreted in the framework of total routhian surface calculations. All three bands are assigned to two-quasi-particle proton configurations at superdeformed shape.

PACS. 21.10.Re Collective levels – 21.60.Cs Shell model – 23.20.Lv Gamma transitions and level energies – 27.50.+e $59 \leq A \leq 89$

1 Introduction

The study of nuclei at superdeformed (SD) shapes has proven an important tool for testing nuclear shell structure. Since SD states were first found in ^{152}Dy [1], large deformations at high spin have been revealed in many nuclides. Today, SD shapes are identified in four principal regions of the nuclide chart, namely for $A \approx 150$ [2], $A \approx 190$ [3], $A \approx 80$ [4,5] and most recently for the $A \approx 60$ region [6,7]. Some nuclides with $A \approx 130$ are also recognised as exhibiting high-spin band structures with features characteristic of superdeformation, but with smaller quadrupole deformations than in the principal regions [8].

This paper reports on an observation of three γ-ray cascades in ^{88}Mo with decay characteristics reflecting collective rotational excitations at SD shapes. By deducing the quadrupole moment Q_t of the strongest band from the residual Doppler shift and assuming a prolate shape, an approximate value of 0.6 is concluded for the quadrupole deformation parameter β_2. Together with the recent discoveries of SD bands in ^{89}Tc [9] and ^{91}Tc [10], this confirms the theoretically predicted [11–14] extension of the $A \approx 80$ SD region into a new region of SD shapes around $A = 90$, further from the line of β-stability. For this new region of SD nuclei, contrary to the $A \approx 80$ nuclei where even the ground states are quite deformed, the states which are yrast at low angular momentum and excitation energy are essentially single-particle-excited states at near-spherical shape. This region of superdeformation is therefore more similar to the heavier A$\approx$ 150 and A$\approx$ 190 SD nuclei.

2 Experiment and analysis

The aim of the present experiment was to investigate the existence of the theoretically predicted [11–14] SD shapes in the neutron deficient $A \approx 90$ region. Excited states in the nuclide ^{88}Mo were populated in the compound nucleus reaction ^{40}Ca+^{58}Ni $\rightarrow$ ^{98}Cd* $\rightarrow$ ^{88}Mo+2α2p. A ^{40}Ca beam of 185 MeV from the 88-Inch Cyclotron of the Lawrence Berkeley National Laboratory was used to bombard a self-supporting ^{58}Ni enriched target foil of thickness 0.38 mg/cm^2. The target was placed at an angle of 30° relative to the beam direction, resulting in an effective thickness of 0.44 mg/cm^2. The detector setup consisted of the GAMMASPHERE detector array [15] with 94 Compton-suppressed germanium spectrometers and the MICROBALL charged particle detector system [16], a 4π array of 95 CsI(Tl) scintillators. With an event trigger requiring coincidences between three or more escape-

[a] *Present address:* Physics Department, Yale University, New Haven, CT 06520-8124, USA
[b] *Present address:* Department of Physics and Astronomy, State University of New York at Stony Brook, Stony Brook, NY 11794, USA

Table 1. The transition gamma energies (in keV) for the three SD bands with uncertainties and the projected angular distribution ratios, $\mathcal{R}$, for the strongest band with uncertainties. The $\mathcal{R}$ values were produced by in the spectra gated by band 1 (using all combinations of double gates in the band) calculating the ratio: $\mathcal{R} = I_{0^\circ,180^\circ}/I_{90^\circ}$ for the peaks in the band. Here, I_{90° is the intensity from detectors at angles around 90 degrees relative to the beam axis and $I_{0^\circ,180^\circ}$ is the intensity from the forward and backward angle detectors. $\mathcal{R}$ is normalised for the number of detectors. Although the errors are rather large, the $\mathcal{R}$ values are consistent with quadrupole transitions, indicating a rotational structure. Assuming a spin alignment factor $\alpha = 0.75$ in the reaction, the expected ratio is 1.3 for a stretched quadrupole transition and 0.7 for a stretched dipole transition [19]. The statistics of bands 2 and 3 were too low for such analysis

E_γ band 1	$\mathcal{R}$ band 1	E_γ band 2	E_γ band 3
1237.6 ± 0.3	$1.1^{+0.3}_{-0.3}$		1260.3 ± 0.5
1342.9 ± 0.2	$1.6^{+0.4}_{-0.3}$		1383.7 ± 0.5
1480.7 ± 0.2	$1.9^{+0.4}_{-0.3}$	1457.7 ± 0.8	1521.3 ± 0.6
1633.7 ± 0.2	$2.1^{+0.5}_{-0.4}$	1596.1 ± 0.8	1670.9 ± 0.6
1795.0 ± 0.2	$1.6^{+0.4}_{-0.3}$	1743.3 ± 0.7	1816.3 ± 0.6
1962.4 ± 0.3	$1.9^{+0.6}_{-0.4}$	1895.4 ± 0.7	1971.1 ± 0.7
2134.2 ± 0.4	$1.0^{+0.8}_{-0.6}$	2050.8 ± 1.3	2134.6 ± 0.7
2305.4 ± 1.3		2228.6 ± 1.2	2298.0 ± 1.4

suppressed Ge detectors, a total number of 2.4×10^9 raw events were collected on magnetic tape.

All collected data were sorted off-line into E_γ–E_γ matrices and E_γ–E_γ–E_γ cubes of the RADWARE types [17], subject to the appropriate charged-particle gates. The $2\alpha 2p$ gate contained contaminants due to other particle channels, mainly ^{87}Nb from the $2\alpha 3p$ channel. These unwanted contributions were subtracted using the corresponding particle-gated matrices. The resulting data consisted of 6.8×10^7 $\gamma\gamma$ and higher-fold coincidence events. Small contributions of ^{88}Zr from the reaction ^{40}Ar+^{58}Ni $\rightarrow$ ^{98}Pd* $\rightarrow$ ^{88}Zr+2α2p were also found, induced by an ^{40}Ar contamination of the beam. The relative intensity of the strongest of these ^{88}Zr transitions is approximately 1% of the strongest ^{88}Mo transitions. From the γ-ray coincidence data in the $2\alpha 2p$ gate leading to ^{88}Mo, three γ-ray cascades of mutually coincident transitions were found, showing the decay characteristics of superdeformed bands.

3 Results

3.1 Identification of bands

Gamma-ray energy spectra gated by transitions belonging to the three SD bands are shown in Fig. 1. The transition energies are tabulated with uncertainties in Table 1. The first cascade (panel **a**) is the most intense, carrying approximately 1% of the intensity flowing through the lowest $2^+ \rightarrow 0^+$ (ground state) transition. The transition energies of this band range from 1238 keV to 2305 keV over 8 observed transitions. The two other SD bands in ^{88}Mo are weaker, of the order of 0.3% relative intensity. Band 2 contains 6 transitions with energies from 1458 keV to 2229 keV and the third cascade has 8 transitions with energies from 1260 keV to 2298 keV. All three bands in Fig. 1 were produced by adding all combinations of double gates in the three- and higher- fold $2\alpha 2p$-gated data. Relevant background contributions were subtracted. The two weaker cascades in Fig. 1 exhibit a pattern of interweaved γ-ray transitions. This suggests that they constitute the two signatures of a strongly coupled band built on a quasi-particle excitation containing a high-Ω particle. Using clean gates in the three bands, the known transitions [18] between the low-lying yrast states of ^{88}Mo, could be observed exclusively. From these results and from the particle coincidences the unambiguous conclusion is that all the three rotational bands belong to the nuclide ^{88}Mo. The projected angular correlations for the γ-rays of the strongest of the three bands are consistent with stretched E2 transitions (Table 1), confirming the collective rotational structure for this band. The entry points for the decay from the SD bands into the low-lying states lie at an angular momentum above $20\hbar$ for all three bands. Strong fragmentation of the decay together with lack of statistics made it difficult to specify the feed-in point with better precision.

3.2 Q_t measurement

In order to confirm the superdeformed shape for the strongest band, the Residual Doppler Shift Technique [20] was used. The two weaker bands had too low statistics for such an analysis. This method is based on the fact that the high spin SD transitions usually are much faster than the low lying yrast sequence and therefore enable extraction of lifetime information also from thin-target data. Due to the large collective E2 transition strengths, the SD states have very short half-lives, and the highest states will decay while the nucleus is still slowing down in the target. The residual Doppler shift due to this deceleration can be measured and described by defining the fractional Doppler shift $F(\tau)$:

$$F(\tau) = v_{SD}(E_\gamma)/v_f.$$

Here, v_f is the average velocity at the point of recoil formation in the target and v_{SD} is the velocity of the recoil nucleus at the time of gamma decay. τ is the time from recoil formation to decay. The $F(\tau)$ values were also calculated using known stopping powers [21]. Side-feeding was modelled in accordance with the experimental intensity profile and assuming a cascade of two transitions (with lifetimes following the same rotational model as the in-band transitions) feeding into each SD state.

By comparing experimental data to these calculated values, the deformation can be estimated. Figure 2 shows the $F(\tau)$ values as a function of transition energy for the strongest SD band of ^{88}Mo. Values for a few low-lying yrast transitions of ^{88}Mo are plotted for comparison. The curves are calculated values for different Q_t. Although lack

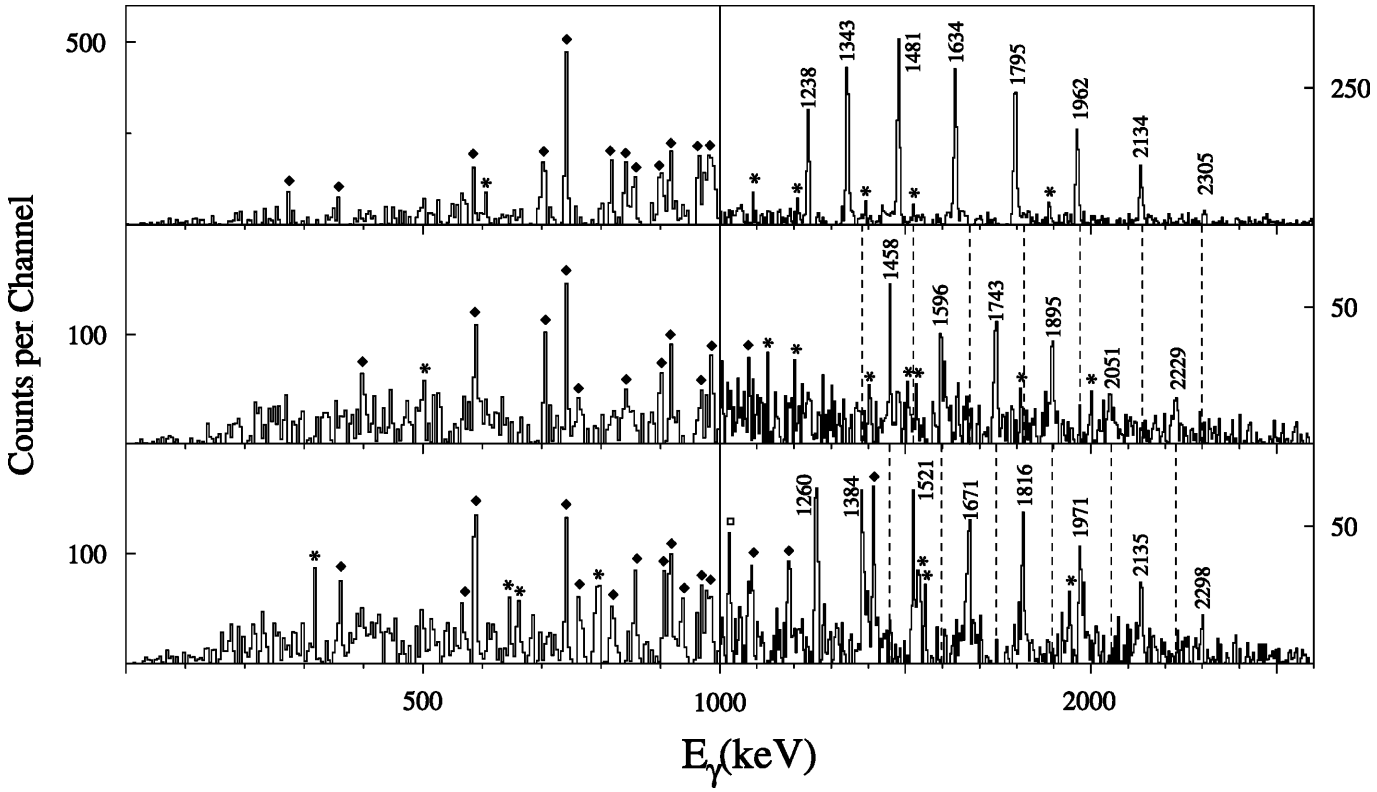

Fig. 1. Gamma-ray energy spectra created by summing coincidence gates set on transitions belonging to the three different SD bands in ^{88}Mo. All three bands are produced by adding all combinations of double gates in the three- and higher- fold $2\alpha 2p$-gated data. Note that that both the x scales and y scales are different for the three bands below and above the break-point at 1000 keV. Relevant background contributions have been subtracted. The dispersion in all spectra is 4 keV per channel. Members of the SD bands are labelled with their γ-ray energies in keV. These transition energies are also tabulated in Table 1 with uncertainties. The transition energies of band 2 are marked with dashed lines in the spectrum of band 3, and vice versa, to emphasise the almost perfectly interweaved transition energies. All three spectra are corrected for the residual Doppler effect using a smooth fit to the $F(\tau)$ values from the strongest band. Peaks that belong to the low-lying yrast transitions of ^{88}Mo [18] are marked by diamond symbols, peaks from unplaced transitions in coincidence with the ^{88}Mo low-lying yrast transitions are marked by stars. One peak at 1025.6 keV (marked by an open square) could not be identified unambiguously. It is clear that the three SD bands belong to the nuclide ^{88}Mo

of statistics makes it difficult to determine the Q_t value with high accuracy, it is clear that this band has a large deformation. The experimental data is best fitted by the value $Q_t = 6.0^{+2.0}_{-1.4}$ eb. The deduced Q_t value corresponds to a quadrupole deformation of $\beta_2 \approx 0.6$, assuming a prolate shape. This confirms the SD nature of this band.

4 Discussion

SD nuclei in the $A \approx 80 - 90$ region have been observed for proton numbers Z=38-41. The shell structure in this mass region can be understood by means of the deformed Woods-Saxon (WS) spectrum [22], Fig. 3. In the subsequent discussion, the same diagram will be used for neutrons since their energy levels are quite similar. For nucleon numbers 38-46 and for deformations ranging from $\beta_2 = 0.40$ to $\beta_2 = 0.75$, there is a region of low level density, where a set of shell gaps appear, ranging from superdeformation ($\beta_2 \approx 0.5$) for nucleon numbers 42 and 44 to enhanced superdeformation ($\beta_2 \approx 0.7$) for nucleon numbers 42 and 46. With respect to the deformed gap at nucleon number 38, two intruder orbitals from the major shell above become occupied at particle number 44 at SD shape, namely the $[431]\frac{1}{2}$ and $[550]\frac{1}{2}$ Nilsson orbitals. The latter will referred to as the $\mathcal{N}$=5 orbital, following the notation of Bengtsson [23]. The expression 5^n referres to a configuration where n particles are put in a $\mathcal{N}$=5 Nilsson orbital and 5_n referres to the n:th $\mathcal{N}$=5 Nilsson orbital.

It is quite instructive to compare the single-particle spectrum of the WS potential with the anisotropic harmonic oscillator (HO). The shell gaps at 2:1 shapes of the HO potential occur at nucleon numbers 28,40,60,80, and 110. This compares rather well with the corresponding gaps in the realistic WS potential where the spin-orbit interaction is included. This suggests that the spin-orbit coupling is less influential for the determination of shell gaps at SD shapes than for a spherical shape. Also the intrinsic structure of the SD states at N,Z=44 in the WS potential is similar to that of the HO potential at N,Z=40. In both potentials, one $\mathcal{N}$=5 orbital is occupied, but an

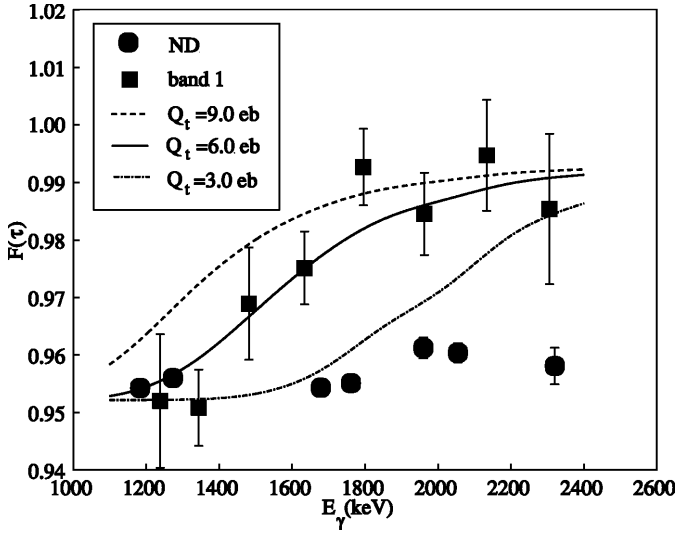

Fig. 2. $F(\tau)$ plotted as a function of γ-ray energy for ^{88}Mo. The data points are derived from the residual Doppler shifts of the γ-ray energies as a function of detector angle relative to the beam. Calculated $F(\tau)$ curves are plotted for different Q_t values. The data for band 1 (filled squares) are in closest agreement with a calculated curve representing a Q_t value of 6.0 eb, indicating a SD shape. The slower low-lying yrast transitions (ND) [18], at 1273, 1679, 1761, 1960, 2055 and 2320 keV, marked by filled circles, lie approximately on a horizontal line. This indicates a much smaller residual Doppler shift as expected for these transitions

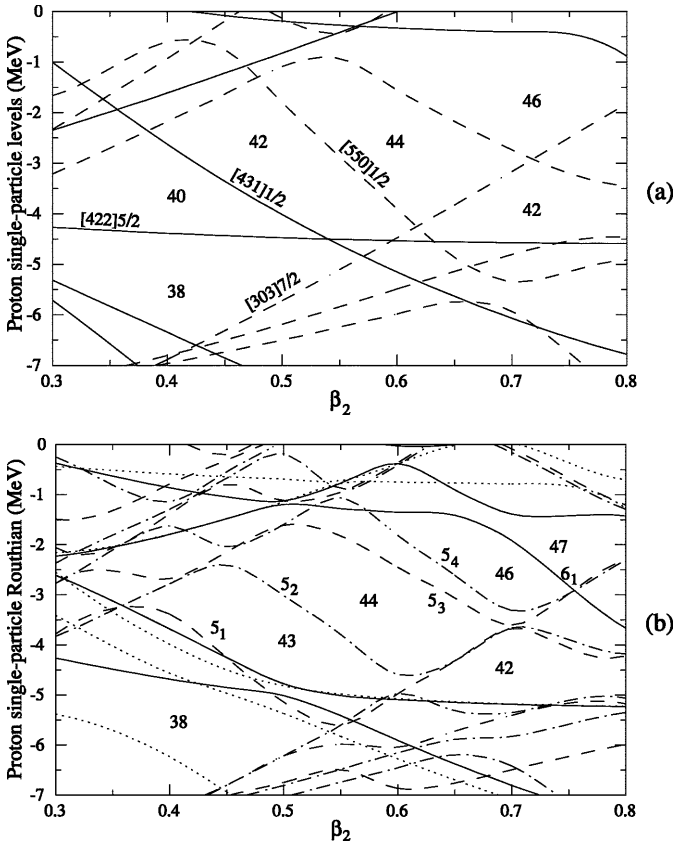

Fig. 3. Panel a: Single-proton diagram of the deformed WS potential for Z=42 as a function of quadrupole deformation. The β_4 deformation was varied with β_2 according to the minimum value obtained for each Z at the corresponding shell gap. Solid:π=+, dashed:π = −. **Panel b:** The same single-proton diagram at a rotational frequency of $\hbar\omega$=0.8 MeV. (π, α): solid=$(+, \frac{1}{2})$, dotted=$(+, -\frac{1}{2})$, dash-dotted=$(-, \frac{1}{2})$, dashed=$(-, -\frac{1}{2})$

additional pair is in the $\mathcal{N}$=3 and $\mathcal{N}$=4 orbitals in the WS potential. Due to the spin-orbit splitting and the flatness of the potential well, the shell gaps in the WS potential are, however, much less pronounced. Hence, instead of the single gap at N,Z=40 there is a region of low level density, see Fig. 3.

As discussed in [24], the shell gaps that occur below the energetically favoured $\Omega = \frac{1}{2}$ intruder orbital, like in the $^{88}_{42}$Mo$_{46}$ case the Z=42 gap below the $\mathcal{N}$=5 orbital, become quenched with increasing frequency due to the strong Coriolis coupling for this orbital. This is illustrated in Fig. 3b, showing the equivalent single-particle spectrum as in Fig. 3a, but at a rotational frequency of $\hbar\omega = 0.8$ MeV. Here, the favoured nucleon numbers become N,Z=43-44 at SD shape and N,Z=42 and 46 at an enhanced SD shape. From this simple diagram, one may therefore expect to find SD rotational bands in $^{88}_{42}$Mo$_{46}$ at very large quadrupole deformation ($\beta_2 \approx 0.65 - 0.70$). Also the nucleus $^{89}_{42}$Mo$_{47}$ appears to have a very favoured enhanced SD shell structure ($\beta_2 \approx 0.70 - 0.75$), where the odd neutron occupies the $\mathcal{N}$=6 $i_{13/2}$ intruder orbital. However, the present calculations do not support that this intruder orbital should be occupied already in the low lying SD structures of $^{87}_{41}$Nb$_{46}$ as reported recently [25].

As seen from Fig. 3, the theoretically predicted 'doubly-magic' SD nucleus in the $A \approx 90$ region is the not yet observed nuclide $^{88}_{44}$Ru$_{44}$ with the configuration $\pi = \nu = 5^2$. Most of the SD nuclei in this mass region have been assigned to the $\pi = 5^1, \nu = 5^2$ configuration. However, recent life-time measurements reveal that e.g. the SD-bands of the Sr isotopes have a smaller deformation than $\beta_2 = 0.5$ [26–28]. Indeed, the extended TRS calculations show that in the yrast bands of the SD Sr-region only one single $\mathcal{N}$=5 neutron orbital is occupied and no $\mathcal{N}$=5 proton orbital. Only for $Z > 38$ does a single $\mathcal{N}$=5 proton orbital become occupied. Again, this can be understood from Fig. 3b, showing the favoured Z=38 and Z=43 gaps separating the 5^0 and 5^1 as well as the 5^1 and 5^2 proton configurations. Excitations across the Z=43 gap are costly in energy for proton numbers Z$\leq$ 43. In $^{83}_{39}$Y$_{44}$, the yrast SD band [29] is assigned to involve the $\pi = 5^1$, $\nu = 5^2$ configuration, similar to $^{84}_{40}$Zr$_{44}$ [28, 30], implying that in the even-even nuclei, one deals with two-quasi-particle proton excitations, which become yrast at SD shape. This is another sign of the lack of very pronounced shell gaps for protons and neutrons. Therefore, the structure of the rotational bands in this mass region is more difficult to determine and a systematic understanding of this mass region is not yet established. To further investigate this SD region towards larger proton numbers

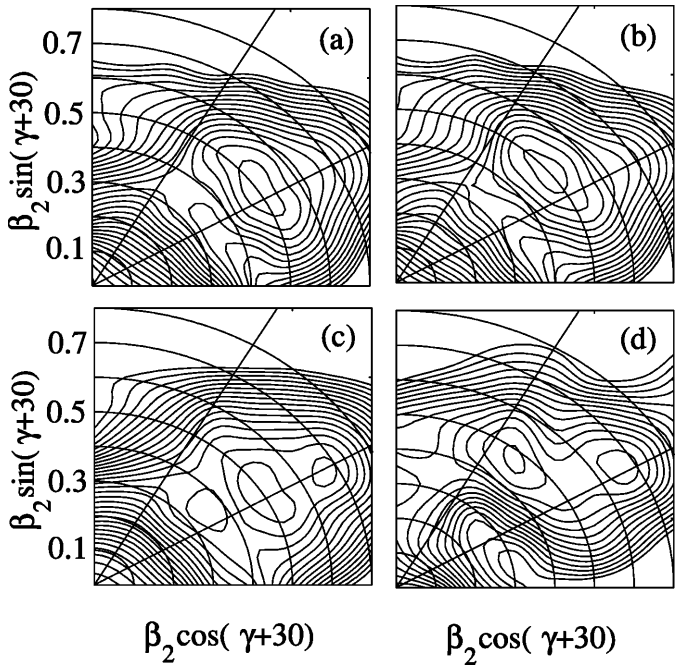

Fig. 4. Calculated total routhian surfaces at $\hbar\omega = 0.8$ MeV (**a,b,c**) and $\hbar\omega = 1.4$ MeV (**d**), based on the $(\pi,\alpha) = (-,0)$ two-quasi-proton configuration (**a**), the $(\pi,\alpha) = (-,1)$ two-quasi-proton configuration (**b**), and the $(\pi,\alpha) = (+,0)_{1,2}$ vacuum configurations (**c** and **d**). The contour interval is 0.5 MeV. In all four cases a well defined minimum around β_2=0.5 occurs. For the vacuum configuration in panel **c** there is in addition an enhanced SD minimum at $\beta_2 \approx$0.65 (The extreme point at $\beta_2 \approx$0.35 in panel **c** is a maximum point.). At higher frequency (**d**) the minimum at $\beta_2 \approx$0.65 becomes more well defined, and the minimum at $\beta_2 \approx$0.5 moves into the γ-plane

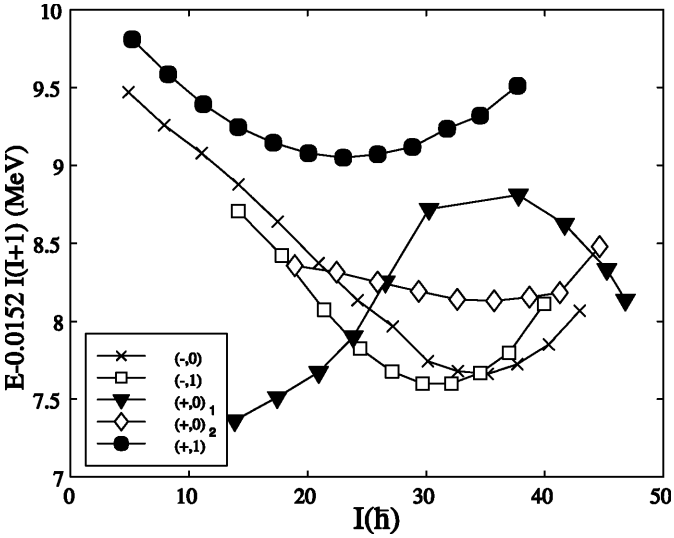

Fig. 5. Energy as a function of spin for some theoretical configurations. The energy is corrected with the energy for a rigid rotor with $\hbar^2/2\mathcal{J} = 0.0152$ MeV, where $\mathcal{J}$ is the moment of inertia. Note that the two vacuum configurations, $(\alpha,\pi) = (+,0)_1$ ($\beta_2 \approx 0.5$) and $(\alpha,\pi) = (+,0)_2$ ($\beta_2 \approx 0.65$), are not the most energetically favoured. Instead, the two excited configurations, $(\alpha,\pi) = (-,1)$ $([431]\frac{1}{2})5^1$ and $(\alpha,\pi) = (-,0)$ $([422]\frac{5}{2})5^1$, are lowest in energy over most of the spin range of interest. In contrast, the $(\alpha,\pi) = (+,1)$ $([303]\frac{7}{2})5^1$ configuration is energetically unfavoured

appears imperative, especially to study the evolution of the proton and neutron shell structure.

For a detailed interpretation of the present data, cranked Strutinsky type calculations based on the WS potential [22,31] have been performed. The pairing interaction was treated self-consistently using both monopole and quadrupole components [32]. In order to avoid the spurious pairing-phase transition, approximate particle number projections using the Lipkin-Nogami approach [32, 33] were performed. Excited quasi-particle configurations are blocked self-consistently. The energy in the rotating frame of reference, is then minimised with respect to the β_2, β_4 and γ deformation parameters for each specified configuration. More details concerning these extended total routhian surface calculations can be found in [34].

The calculations predict favourable configurations at both SD shape ($\beta_2 \approx 0.5$) and enhanced SD shape ($\beta_2 \approx 0.65$). Selected calculated total routhian surfaces for the nucleus ^{88}Mo are shown in Fig. 4. The quenching of the Z=42 SD gap with frequency and the large alignment of the 5_1 orbital favours particle-hole excitations from the $\mathcal{N}$=3 and $\mathcal{N}$=4 orbitals into the 5_1 orbital. Indeed, the calculations show, that different two-quasi-particle proton configurations are lower in energy than the zero quasi-particle configurations, $(+,0)_{1,2}$, in a spin range of 20-40$\hbar$, Fig. 5. Note also, that the enhanced SD structure, $(+,0)_2$, is lower in energy than the SD structure, $(+,0)_1$, in roughly the same spin region. At a deformation of $\beta_2 = 0.5$ the proton excitations from the $[422]\frac{5}{2}$ and $[431]\frac{1}{2}$ orbitals into the 5_1 orbital were calculated to be lowest in energy, Fig. 6. The two-quasi-particle excitation from the $[303]\frac{7}{2}$ Nilsson orbital into the 5_1 orbital favours a larger deformation ($\beta_2 \approx 0.6$). However, these positive parity configurations cannot compete in energy with the negative parity $([431]\frac{1}{2})5^1$ configuration, Fig. 5. Due to the large signature splitting of the $[431]\frac{1}{2}$, orbital, only the lowest signature is expected to receive significant feeding, i.e. the $(\pi,\alpha) = (-,1)$ branch. Hence, the most intense observed SD band (band 1) is assigned to that configuration. The calculation predicts a non negligible γ-deformation, starting out at spin 15$\hbar$ with $\beta_2 = 0.51$ and $\gamma \approx 10°$ and moving towards $\beta_2 = 0.47$ and $\gamma \approx 17°$ at spin 41$\hbar$. The calculated dynamical $\mathcal{J}^{(2)}$ moment of inertia agrees fairly well with the experimental results, Fig. 7, rendering further support to the assignment. Fig. 7 shows the dynamical moments of inertia($\mathcal{J}^{(2)}$) plotted for the three experimentally observed bands as well as for a number of calculated configurations. Note that the neutron configuration is stable over the frequency range of interest, having two $\mathcal{N}$=5 high-j orbitals occupied. At the same deformation parameters as above, $\beta_2 \approx 0.5$, $\gamma \approx 10°$, the neutron shell gap for N=46 is about 1 MeV.

The $([422]\frac{5}{2})5^1$ configuration is less γ-driving and also has a slightly larger quadrupole deformation ($\beta_2 = 0.52$ at

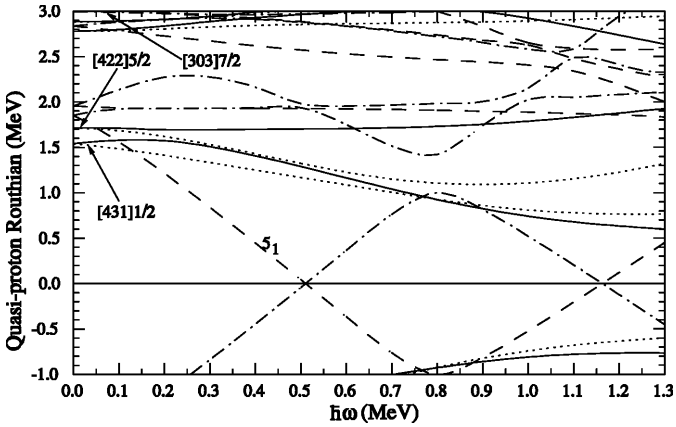

Fig. 6. Theoretical quasi-proton routhians for a WS potential as a function of rotational frequency. The deformation parameters are chosen as ($\beta_2 = 0.50, \beta_4 = 0.030, \gamma = 10.4°$). Note that although the two interactions between the $\alpha = +\frac{1}{2}$ ($\alpha = -\frac{1}{2}$) $[422]\frac{5}{2}$ orbital and the $\alpha = +\frac{1}{2}$ ($\alpha = -\frac{1}{2}$) $[431]\frac{1}{2}$ orbital at $\hbar\omega \approx 0.25$ ($\hbar\omega \approx 0.6$) complicates the picture somewhat, the splitting of the $[422]\frac{5}{2}$ orbital remains small over the whole frequency range, with a maximum of less than 200 keV at $\hbar\omega$=1.3. The splitting of the $[431]\frac{1}{2}$ orbital, on the other hand, is large over the entire range of frequencies. (π, α): solid=$(+, \frac{1}{2})$, dotted=$(+, -\frac{1}{2})$, dash-dotted=$(-, \frac{1}{2})$, dashed=$(-, -\frac{1}{2})$

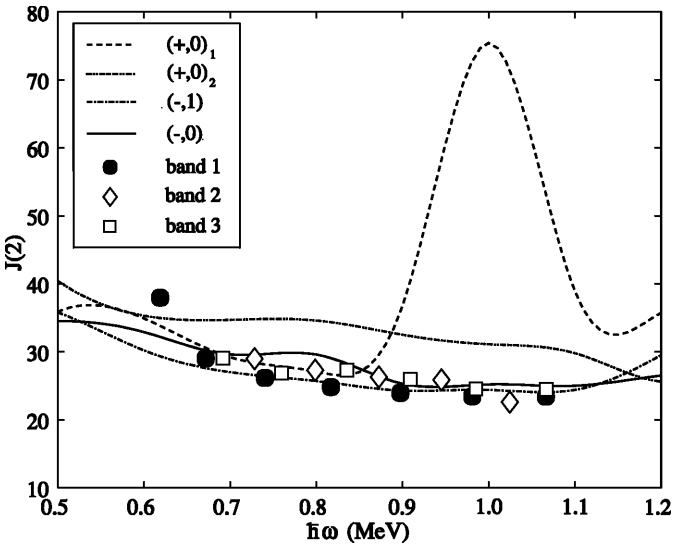

Fig. 7. Experimental dynamical moments of inertia $\mathcal{J}^{(2)}$ (symbols) for the three bands compared to values from the cranked Strutinsky calculation (lines). The experimental data correspond better to the $(\pi, \alpha) = (-, 1)$ and $(-, 0)$ (proton excitation) configurations (both with $\beta_2 \approx 0.5$) than to the two vacuum configurations $(+, 0)_1$ ($\beta_2 \approx 0.5$) and $(+, 0)_2$ ($\beta_2 \approx 0.65$)

$\hbar\omega = 0.4$ MeV). For this band structure, both signatures are expected to be seen in the experimental data, i.e. the $(\pi, \alpha) = (-, 0)$ and $(\pi, \alpha) = (-, 1)$ branches.

In the present TRS-model, only the lowest 2-quasiparticle states of each signature and parity can be calculated self-consistently. For the negative parity side-bands based on proton configurations, states with signature $\alpha = 1$ and $\alpha = 0$ were calculated. Due to the large signature splitting of the $[431]\frac{1}{2}$ Nilsson orbit (see Fig. 6), the $(-, 1)$ configuration correspond to the $([431]\frac{1}{2})5^1$ configuration, whereas the $(-, 0)$ configuration is of $([422]\frac{5}{2})5^1$ character. These two configurations can be rather clearly separated on the two different surfaces. The $(-, 1)$ signature partner of the $([422]\frac{5}{2})5^1$ configuration will be the first excited surface with this signature, but is at present not calculated. The calculated $(-, 0)$ surface will therefore be used to describe both signatures of the $([422]\frac{5}{2})5^1$ configuration. Since this orbital exhibits rather modest signature splitting, these two signature are not expected to behave very differently. This small signature splitting is in agreement with the experimental observations of bands 2 and 3. The small signature splitting of the $([303]\frac{7}{2})$ orbital makes also the $([303]\frac{7}{2})5^1$ configuration a possible candidate, but this configuration is energetically unfavoured (Fig. 5), so the more likely assignment for bands 2 and 3 is the $([422]\frac{5}{2})5^1$ configuration.

The calculated $\mathcal{J}^{(2)}$ moments of inertia for the suggested configuration $(-, 1)$ coincide with the experimental values for bands 2 and 3, see Fig. 7. With increasing spins, also this configuration is calculated to move into the γ-plane. The energy surface is quite soft in the γ-direction and one may expect low lying γ-vibrational bands at SD shapes or that the coupling to the γ-vibrations may play a role for the SD spectra. However, the present set of data does not allow for a more complete study of the SD structures, due to the intensity limitation.

Figure 7 also shows the calculated $\mathcal{J}^{(2)}$ moments of inertia for the SD and enhanced SD bands, based on the vacuum configurations. The presence of the large Z=42 gap in combination with the strong Coriolis coupling of the high-j $\mathcal{N}$=5 orbital, results in a pronounced band crossing for the SD $(+, 0)_1$ configuration. Since the moments of inertia of the observed bands are rather flat, this confirms the assignments to two-quasi-particle excitations for all three bands. The enhanced SD structure, $(+, 0)_2$ lacks the band-crossing, due to larger deformation and no change in the intrinsic structure. Note also that at the larger deformation, another pair of $\mathcal{N}$=5 neutrons are occupied, see Fig. 3. Still, the calculated larger value of $\mathcal{J}^{(2)}$ for this configuration does not support such an interpretation of the yrast band (Fig. 7). Hence, both energy considerations and the dynamical moments of inertia speak in favour of the assignments. Based on the calculations the lowest observed state in band 1 is tentatively assigned to I=21$\hbar$, implying that the highest spin observed in the present data is I=39$\hbar$.

5 Conclusion

In summary, three discrete-line superdeformed bands in ^{88}Mo at high angular momenta have been identified. The large value of the experimentally deduced quadrupole moment for the most intense band ($Q_t = 6.0^{+2.0}_{-1.4}$) provides evidence that these structures indeed correspond to superdeformed shapes, with a quadrupole deformation of

$\beta_2 \approx 0.6$. In comparing the data to mean field model calculations, it was found that all three bands can be interpreted as two-quasi-proton configurations at SD shape.

The authors are grateful to Prof. H. Grawe for providing the targets. The staff and crew of the LBNL 88-Inch Cyclotron are thanked for their competent and dedicated operation. Dr. D.C. Radford is thanked for the use of the RADWARE codes. This work was supported by the Swedish Natural Science Research Council and the U.S. Department of Energy; grant No. DE-FG05-88ER40406 (Washington University) and contract No. DE-AC03-76SF00098 (LBNL).

References

1. P.J. Twin et al. *Phys. Rev. Lett.*, **57**(7), 811–814 (1986)
2. P.J. Nolan and P.J. Twin. *Ann. Rev. Nucl. Part. Sci.*, **38**, 533 (1988)
3. R.V.F. Janssens and T.L. Khoo. *Ann. Rev. Nucl. Part. Sci.*, **41**, 321–355 (1991)
4. C. Baktash et al. *Phys. Rev. Lett.*, **74**(11), 1946–1949 (1995)
5. D.R. LaFosse et al. *Phys. Lett. B*, **354**(1,2), 34–40 (1995)
6. C.E. Svensson et al. *Phys. Rev. Lett.*, **79**(7), 1233–1236 (1997)
7. C.E. Svensson et al. *Phys. Rev. Lett.*, **82**(17), 3400–3403 (1999)
8. R. Wyss et al. *Phys. Lett. B*, **215**(2), 211–215 (1988)
9. B. Cederwall et al. *Euro. Ph. Journ. A*. Accepted for publication
10. E. Ideguchi et al. To be published.
11. T. Werner, J. Dudek and L.L. Riedinger. *Phys. Lett. B*, **211**(3), 252–258 (1988)
12. I. Ragnarsson. In *Proc. Workshop on the science of intense radioactive ion beams*, page 199, Los Alamos, 1990
13. R. Wyss. In *Euroball Users Meeting*, Strasbourg, 1994. slide report
14. A.V. Afanasjev and I. Ragnarsson. *Nucl. Phys. A*, **586**(3), 377–395 (1995)
15. I.-Y. Lee. *Nucl. Phys. A*, **520**, 641c–655c (1990)
16. D.G. Sarantites et al. *Nucl. Instr. and Meth. A*, **381**(2,3), 418–432 (1996)
17. D.C. Radford. *Nucl. Inst. and Meth. A*, **361**, 297–305 (1995)
18. M. Weiszflog et al. *Z. Phys. A*, **342**(3), 257–265 (1992)
19. Krane et al. *Nucl. Data Tables*, **11**, 351 (1973)
20. B. Cederwall et al. *Nucl. Instr. and Meth. A*, **354**(2,3), 591–594 (1995)
21. J.F. Ziegler et al. Volume 1. Pergamon, London, 1985
22. S. Ćwiok et al. *Comp. Phys. Comm.*, **46**, 379 (1987)
23. T. Bengtsson et al. *Phys. Lett. B*, **208**(1), 39–44 (1988)
24. R. Wyss et al. *Nucl. Phys. A*, **511**(2), 324–344 (1990)
25. D.R. LaFosse et al. *Phys. Rev. Lett*, **78**(4), 614–617 (1997)
26. M. Devlin et al. *Phys. Lett. B*, **415**(4), 328–334 (1997)
27. C.-H. Yu et al. *Phys. Rev. C*, **57**(1), 113–122 (1998)
28. F. Lerma et al. to be published
29. C. Baktash. In *Proceedings of the Conference on Nuclear Structure at the Limits, ANL/PHY-97/1*, pages 90–98. Argonne National Laboratory, Argonne, Illinois, USA, 1996
30. H.-Q. Jin et al. *Phys. Rev. Lett.*, **75**(8), 1471–1474 (1995)
31. R. Wys, W. Nazarewicz and A. Johnsson. *Nucl. Phys. A*, **503**(2), 285–330 (1989)
32. W. Satula et al. *Nucl. Phys. A*, **578**(1), 45–61 (1994)
33. Y. Nogami, H.C. Pradhan and J. Law. *Nucl. Phys. A*, **201**(2), 357–368 (1973)
34. W. Satula and R. Wyss. *Phys. Script.*, **T56**, 159–166 (1995)